communications earth & environment

Article

https://doi.org/10.1038/s43247-024-01491-8

Dual clumped isotopes from Mid-Eocene bivalve shell reveal a hot and summer wet climate of the Paris Basin

Jorit F. Kniest[1] ✉, Amelia J. Davies[1], Julia Brugger[2], Jens Fiebig[1], Miguel Bernecker[1], Jonathan A. Todd[3], Thomas Hickler[2], Silke Voigt[1], Alan Woodland[1] & Jacek Raddatz[1,4]

Accurate reconstruction of seasonal atmospheric patterns of the past is essential for reliable prediction of how climate will evolve due to anthropogenic CO_2 forcing. The Eocene 'hot house' climate, as the warmest epoch during the Cenozoic, is considered as a potential analogue for 'high-CO_2' future climate scenarios. In this context, the reconstruction of variations in seasonality are as important as changes in mean annual conditions. Here we combine stable oxygen ($\delta^{18}O$) and dual clumped isotope ($\Delta_{47} + \Delta_{48}$) measurements of a bivalve shell to determine sub-annual variations in sea surface temperatures and oceanic freshening in the Paris Basin during the Mid-Eocene Climate Optimum, 40 million years ago. Our reconstruction indicates to high mean annual temperatures with a small seasonal amplitude (33.3 °C ± 4.4 °C) and an enhanced fresh water input during the summer period. Our results implying a substantially warmer climate state with different hydrological conditions for Western Europe during the Eocene than previously suggested by proxy data or climate modelling.

The Eocene has drawn attention as a potential analogue for 'high-CO_2' future climate scenarios[1], as this period shows the highest atmospheric temperatures and pCO_2 during the Cenozoic[2]. Furthermore, the Eocene is characterised by recurring hyperthermals, for example the Palaeocene-Eocene Thermal Maximum (PETM) and Mid-Eocene Climate Optimum (MECO), which are comparatively short intervals (10 s to 100 s ka) with rapid changes in temperature and CO_2 concentration in the atmosphere and oceans[2]. Understanding differences in seasonality in such dynamic past warm climates is an important aspect for predicting future climate scenarios[1,3,4].

Due to their sensitive response to short-term atmospheric circulations, shallow marine environments, such as marginal seas, are important targets to reconstruct seasonal patterns in temperature and the hydrological cycle. Analysis of the stable oxygen isotope composition of marine carbonate ($\delta^{18}O_C$) is commonly used to reconstruct annual variability of sea surface temperatures (SST) or salinity changes induced by a variations in fresh water input and evaporation[5–11]. However, accurate reconstructions rely on accurate knowledge of the oxygen isotope composition of the sea water ($\delta^{18}O_{SW}$). The evolution of $\delta^{18}O_{SW}$ during the Cenozoic is relatively well understood regarding long-term variations on global scales, like for open and deep ocean settings[12–14]. In marginal seas, however, only sparse information is available about the oxygen isotope composition of sea water and its seasonal scale dynamics[7,15].

A major step towards more reliable temperature reconstructions was made by the invention of the clumped isotope (Δ_{47}) thermometer. Here, the Δ_{47} represents the temperature-dependent abundance of the ^{18}O-^{13}C-^{16}O isotopologue in CO_2 derived from phosphoric acid digestion of carbonate relative to its stochastic distribution. Since this value addresses the internal fractionation of carbon and oxygen isotopes amongst carbonate isotopologues, its measurement enables reconstruction of carbonate formation temperature independent of $\delta^{18}O_{SW}$. However, if carbonate precipitation occurs faster than isotopic equilibration of dissolved inorganic carbon species, kinetic isotope effects can impact Δ_{47} value in addition to temperature. Through the additional analysis of Δ_{48} (i.e., abundance of ^{18}O-^{12}C-^{18}O isotopologue relative to its stochastically predicted abundance) can be employed to identify the influence of such processes on Δ_{47} and to correct the carbonate formation temperature for kinetic baises[16–19].

Here we combine seasonally resolved stable oxygen and seasonally targeted dual-clumped isotope ($\Delta_{47} + \Delta_{48}$) measurements to reconstructed mean warm and cold season SSTs for the Paris Basin during the Middle Eocene. In addition, clumped-derived temperatures in combination with $\delta^{18}O_C$ are utilised to calculate inter-annual $\delta^{18}O_{SW}$ variability to detected hydrological dynamics, i.e., enhanced fresh water influx or evaporation. Analysis were carried out on one pristine preserved specimen of the bivalve species *Venericor planicosta* from the geological site "Le Guépelle", which consists of shallow marine sediments of the early Bartonian including the

[1]Institute for Geoscience, Goethe-University, Frankfurt a.M., Germany. [2]Senckenberg Biodiversity and Climate Research Centre (SBiK-F), Frankfurt a.M., Germany. [3]The Natural History Museum, London, UK. [4]GEOMAR Helmholtz Centre for Ocean Research Kiel, Kiel, Germany. ✉e-mail: kniest@em.uni-frankfurt.de

MECO (40–39 Ma)[20,21]. In addition, proxy derived reconstructions are compared to published climate model data using the Community Earth System Model (CESM)[22].

Results

Stable oxygen isotopes

The seasonal stable isotopic record obtained from the *V. planicosta* specimen encompasses about seven years and a total range from −6.20‰ to −2.72‰ (Fig. 1). Seasonal $\delta^{18}O_C$ variations were determined by analysing the inner shell aragonite in the direction of growth along four planes, which were cut parallel to the maximum growth axis of the bivalve shell. These four isotopic records cover overlapping growth increment intervals (PBB1 to PBB4, Supplementary Data 2). Applying a general growth model of the shell to the four plane records enables them to be linked to generate a master record (Supplementary Fig. S1). The master record reveals only slight divergence in the variation of isotopic composition of the individual plane records, exhibit a homogenous lateral isotopic distribution through the inner shell. In general, variations between the plane records are within analytical error or based on minor growth model mismatches. The comparison of the master record $\delta^{18}O_C$ values with those measured in the hinge plate shows a similar pattern, which further reveals no major isotopic variability between the different shell parts (Supplementary Fig. S1).

The master record reveals an almost sinusoidal shaped trajectory, suggesting shell accretion during the whole year. However, the peak widths differ between the isotopically lighter and heavier parts of the record, displaying more narrow peaks for the heavy values while the lighter peaks are broader. The cuspate pattern in peak shape might hint to a variable annual growth rate with more reduced growth during the colder months of the year[3]. Full winter growth cessation can most likely be excluded, as growth bands appear shortly before or during periods with the most negative $\delta^{18}O_C$ values and presumably the highest water temperatures, assuming $\delta^{18}O_C$ is primarily controlled by temperature. Thereby, growth band positions point to the initiation of a new increment during spring or early summer times.

To reduce potential growth-related influences on the obtained isotopic data, a non-linear regression model was computed by fitting a sinusoidal function to the master record (s. "Methods"). The model-fit encompasses a peak-to-peak amplitude of 2.4‰ (A) with a mean position of −4.7‰ (M) and ranging from −5.9‰ to −3.5‰ (Fig. 1).

Ten positions along the last four years of the master record were selected for the dual clumped isotope analysis (Supplementary Fig. S1). The material of each five positions were pooled together to obtain the necessary sample size, resulting in two bulk carbonate samples, aimed to represent the isotopically lightest (BL) and heaviest (BH) part, respectively, the coldest and warmest time of the observed seasonal record. Based on control samples, measured parallel to the dual clumped sampling, the calculated weighted average $\delta^{18}O_C$ of the two bulk samples is −5.37 ± 0.45‰ (2σ) for BL_{WA} and −4.03 ± 0.46‰ (2σ) for BH_{WA} (Table 1). These values are within the previously observed isotopic range derived from the model-fit (Fig. 1). However, the difference between BH_{WA} and BL_{WA} of 1.34‰ resolves only about half of the annual isotopic amplitude derived from the model-fit. This results from the lower sampling resolution introduced by the limitation of drilling precision and the required sample size. The two bulk samples therefore rather represent a mean for the warmer and colder season instead of the intended annual extrema.

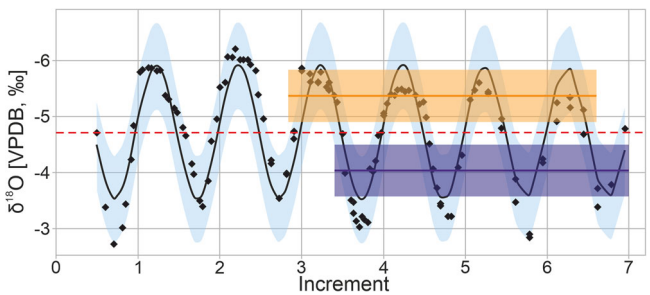

Fig. 1 | Compiled stable oxygen isotope shell record. $\delta^{18}O$ values (black diamonds) as obtained from shell sections PBB1 to PBB4 (Supplementary Data 2 & Supplementary Fig. S1). The blue line represents the fitting curve of the non-linear regression model and the corresponding 95% confidence interval (light blue shaded area). Red dashed line displays mean position of the model fit at −4.7‰. The coloured boxes show the weighted averages (±2σ) for the two bulk samples (BL_{WA} – orange, BH_{WA} - dark blue) at their sampling positions over the last four increments of the obtained record.

Dual clumped isotopes

The results of dual clumped analyses of the two bulk samples and simultaneously measured $\delta^{18}O$ values are compiled in Table 1. The *measured* $\delta^{18}O_C$ values of BL_M and BH_M exhibits close to equal values to the prior calculated BL_{WA} and BH_{WA}, deviating by about 0.1‰.

In contrast to the distinct difference in the stable oxygen isotope composition of the two bulk samples (1.34‰), the Δ_{47} values of BL (0.569‰ ± 0.008) and BH (0.575‰ ± 0.009) deviate by only 0.006‰ (Table 1). Both samples show the same value in Δ_{48} (0.255‰ ± 0.026). A two-sided t-test shows that the Δ_{47} values of BL and BH cannot be statistically distinguished from each other ($t(11) = -1.4729$, $p = 0.1688$). This is reflective of the small difference in clumped isotope composition between BL and BH and comparatively large propagated errors (2SE) of ~0.008‰ for Δ_{47} and ~0.026‰ for Δ_{48} (Table 1), which derived from combined analytical and calibration uncertainties (Table 1).

To detect potential kinetic effects in their isotopic composition, BL and BH are plotted in dual clumped isotope space and are compared to the positions of the $\Delta_{47} + \Delta_{48}$ equilibrium calibration of Fiebig et al.[23](Fig. 2). The offset in Δ_{48} from the calibration line is 0.022‰ for BL and 0.019‰ for BH, respectively, within the propagated error of ~0.026‰ for Δ_{48}. Both measurements intersect the equilibrium calibration within their twofold standard errors, implying that the measured $\Delta_{47} + \Delta_{48}$ values are statistical indistinguishable from equilibrium. For this reason, Δ_{47} values are interpreted to be unaffected by kinetic limitations during mineral formation and, thus, reflecting the formation temperature of the carbonate.

Discussion

Shell isotopic composition

With a total range of 3.5‰ and values from −6.2‰ to −2.7‰ in $\delta^{18}O_C$, the examined specimen in this study has an exceptionally light oxygen isotopic composition and large isotopic variability in comparison to other carbonate shells for the Middle Eocene in the Paris Basin. Previous studies yield annual amplitudes of ~2.0‰ and ranged from about −4.0‰ up to 2.0‰[5,6,9,20,24]. Heaviest $\delta^{18}O_C$ values were obtained for marine gastropods[5,25], which have a vagile mode of life potentially pointing to change in habitats during the year, in contrast to sessile living bivalves. Huyghe et al.[20] analysed gastropod and oyster shells for their isotopic composition throughout the Eocene in the Paris Basin, observing a range of −2.5‰ to −3.1‰ in mean $\delta^{18}O_C$ for specimens from Le Guépelle, distinctly heavier than the mean $\delta^{18}O_C$ of −4.7‰ derived from the non-linear regression model.

In contrast to the taxa analysed in the aforementioned studies, bivalves of the genus *Venericor* have been found to exhibit $\delta^{18}O_C$ values from −6.0‰ to −0.5‰ and annual ranges >2.0‰. Ivany et al.[7] examined a *Venericor* shell from the early Eocene of Alabama, yielding $\delta^{18}O_C$ from −6.4‰ to −1.3‰, similar to the specimen in our study, linking the negative values to reoccurring freshening of the Gulf of Mexico. Sessa et al.[26] reported *Venericor* species occurrences along the whole coast of the Gulf of Mexico in the early Eocene, thriving in full marine to brackish settings. Measured decreases in shell $\delta^{18}O_C$ values are interpreted as reflecting influxes of fresh water and are accompanied by a gradual change in the surrounding sediment assemblage from an offshore to a lagoon system[26]. Similar nearshore habitats with very shallow water depths are also found for *Venericor* species for the southern Paleo North Sea during the Eocene[27]. *Venericor* species, therefore, appear to tolerate environments with an appreciable input of fresh water, i.e. with variable salinities and recording this freshening in their

Table. 1 | Stable Oxygen and dual clumped isotope composition of the bulk samples

	Weighted average		Dual clumped isotope measurments										
							Errors (2SE)			Errors (2SE)			
Sample	Amount of subsamples	δ18O [VPDB, ‰]	2σ	δ18O [VPDB, ‰]	2σ	Δ47[CDES90, ‰]	Analytical	Calibration	Propagated	Δ48[CDES90, ‰]	Analytical	Calibration	Propagated	Replicates
BL	5	−5.37	0.46	−5.25	0.07	0.569	0.0069	0.005	0.0085	0.2558	0.0228	0.01	0.0251	7
BH	5	−4.03	0.46	−3.94	0.16	0.575	0.0074	0.0051	0.0089	0.2557	0.0246	0.01	0.0267	6

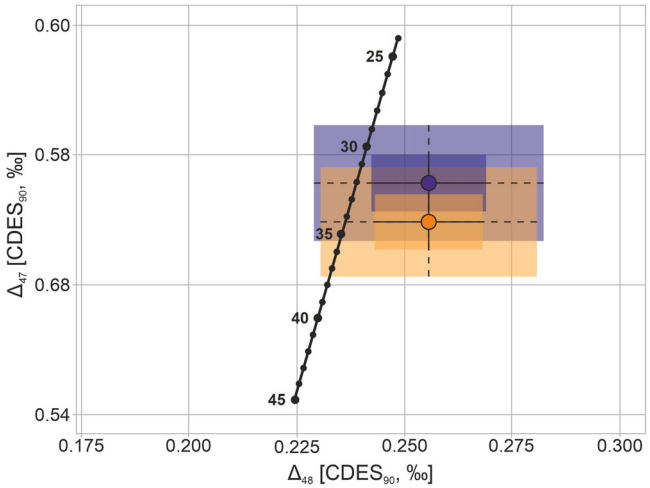

Fig. 2 | Dual clumped isotopic composition of the two bulk samples. Dual clumped values for BL (orange) and BH (dark blue) are displayed in relation to the abiotic equilibrium calibration for $\Delta_{47} + \Delta_{48}$ of Fiebig et al.[23]. Propagated errors are shown as 68% (solid line) and 95% (dashed line) confidence intervals.

isotopic shell record, while accompanied taxa potentially changed their habitat (gastropods) or reacted with growth slowdown or cessations (bivalves).

Temperature conversion of isotopic data

There are several empirically derived relationships to describe the temperature dependent oxygen isotope fractionation between carbonate and water. These may be group-specific, species-specific or based on synthetic carbonates. Application of the appropriate empirical relationship for taxonomic class and mineralogy is fundamental to the derivation of accurate carbonate formation temperature (i.a.[28–31]). For aragonitic bivalves, like *V. planicosta*, the $\delta^{18}O$-temperature calibrations published by Grossman and Ku[28] in the modified version of Dettmann et al.[29] and the $\delta^{18}O$-temperature calibrations introduced by Kim et al.[30] are commonly used for the paleotemperature reconstruction[8,9,24,32]. Determination of temperature depends on both, measured $\delta^{18}O_C$ values and an a priori assumption of the isotopic composition of the ambient seawater. A global $\delta^{18}O_{SW}$ value between −1.0‰ and −0.75‰ is generally applied for the Eocene, suggesting non or negligible polar ice caps[12–14,33]. This range in $\delta^{18}O_{SW}$ is also commonly applied for the Paris Basin in recent studies[6,9,20,24]. In this study, sea surface temperatures (SST) were calculated utilising the fractionation factors of Dettman et al.[29] and Kim et al.[30] and $\delta^{18}O_{SW}$ values (−1.0‰, −0.75‰), to gain insight into how the choice of calibration and variation in $\delta^{18}O_{SW}$ affects the temperature reconstruction.

Seasonal $\delta^{18}O$-derived temperatures ($T_{\delta 18O}$) are obtained by iterating the mean position (M) and the peak-to-peak amplitude (A) of the model-fit through the different $\delta^{18}O$-temperature calibrations and $\delta^{18}O_{SW}$ values. Resulting mean annual temperature (MAT) are 41.1 °C for Dettman et al.[29] and 36.4 °C for Kim et al.[30] with a mean annual range of temperature (MART) of 14.6 °C and 13.0 °C, respectively. Applying the same method to the weighted averages (±2σ) of the bulk samples gives a smaller temperature range of 37.2 °C (±2.8 °C) and 32.9 °C (±2.5 °C) for the winter (BH_{WA}) and 44.6 °C (±2.9 °C) and 40.8 °C (±2.5 °C) for the summer (BL_{WA}) using either Dettmann et al.[29] or Kim et al.[30], respectively. Comparing the resulting temperatures in dependence on the chosen calibrations and $\delta^{18}O_{SW}$, reveals an average offset of ~4.7 °C between the two $\delta^{18}O$-temperature calibration and ~1.4 °C for the different $\delta^{18}O_{SW}$ values (Supplementary Fig. S2, Supplementary Data 4 and 6).

Clumped isotope based temperatures ($T_{\Delta 47}$) are reported for bulk samples BL and BH. As dual clumped isotope analysis indicates that *V. planicosta* precipitates in clumped isotope equilibrium, the Δ_{47} values do not need to be corrected for kinetic effects. Translating the Δ_{47} values (±2SE)

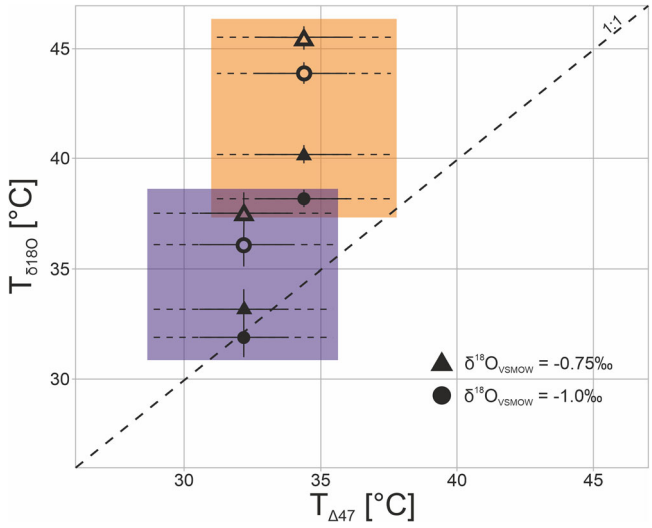

Fig. 3 | Comparison of reconstructed water temperatures from stable and clumped isotopes. $\delta^{18}O$ values of the two bulk samples BL (orange box) and BH (dark blue box), which were simultaneous measured to the clumped isotopes, are converted to temperature values and compared to Δ_{47}-derived temperatures. Temperature conversion of the stable oxygen isotope values are performed by utilising different calibration factors for carbonate-water-fractionation (Dettmann et al.[29] – open symbols, Kim et al.[30] – filled symbols). In addition, $T_{\delta 18O}$ is displayed for two different $\delta^{18}O_{SW}$, which are commonly used form temperature reconstruction for the Eocene Paris Basin[5,6,9]. Propagated errors for the reconstructed temperatures relate to the 68% (solid line) and 95% (dashed line) confidence intervals for Δ_{47} and twofold standard deviation for $\delta^{18}O$ (Table 1). The dashed black line indicates the proposed 1:1-relationship between the two proxy reconstructions.

into temperatures, using the calibration of Fiebig et al.[23], yields $T_{\Delta 47}$ of 34.4 °C (±3.2 °C) for BL and 32.2 °C (±3.3 °C) for BH. Both temperatures are indistinguishable within error.

Seasonal temperature variations

The $\delta^{18}O_C$-derived temperature seasonality is considerably higher than the annual temperature variations inferred by Δ_{47}. The $T_{\delta 18O}$ values of the non-linear regression model gives a MAT of 36.4 °C to 41.1 °C and a MART of ~14 °C. Although *Venericor* specimens from the Eocene Mexican Gulf Coast would suggest the same ambient temperatures, based on a similar isotopic composition to our specimen, this range in temperature values is neither reflective of supposed Eocene climate conditions nor would it appear likely that any shallow-marine organisms would survive in such an environment[7,8]. The $T_{\Delta 47}$ values show a mean of 33.3 °C and a temperature range of 8.7 °C, considering maximum range in the observed errors of the Δ_{47} measurements. However, this range only displays a minimum estimate of the seasonal temperature variation, i.a. due to potentially lower growth rates during the colder season indicated in the cuspate pattern in $\delta^{18}O_c$, which could bias winter temperatures to higher values.

Irrespective of this, the $T_{\Delta 47}$ values are colder and less variable than $T_{\delta 18O}$, although they are on the high end of the temperature range previously reported for the southern Paleo North Sea during the Middle Eocene and the MECO, respectively[9,20,34]. Water temperature reconstructions based on mollusc shell $\delta^{18}O_C$ yield values from 14 °C to 32 °C and an average annual amplitude of ~10 °C for the Middle Eocene in the Paris Basin[5,6,9]. We recalculated mean SST for Le Guépelle from $\delta^{18}O_C$ of the gastropods and oyster shell using the corresponding local $\delta^{18}O_{SW}$ (0.7‰, VSMOW) reported by Huyghe et al.[20]. The recalculation was conducted by employing the previously reported $\delta^{18}O$-temperature calibrations of Dettmann et al.[29] and Kim et al.[30] for the aragonitic gastropods, respectively, the calibration of Daëron et al.[31] for the calcitic oyster shell, to ensure comparability between the previously measured data set and our results. Translating $\delta^{18}O_C$ values of the gastropods and oyster shell from Le Guépelle into water temperatures yields a range of 25.9 °C to 32.0 °C (Supplementary Data 5). Marchegiano and John[34] reconstructed temperatures for the Hampshire Basin from clumped isotope measurements of gastropod shells, revealing a range from 14 °C to 35 °C during the early Bartonian. The authors[34] link these large range to sea-level variations with the highest temperatures occurring during the lowest sea level and the potential formation of a strong summer thermocline.

The comparison of $T_{\Delta 47}$ of BH and BL with their corresponding $T_{\delta 18O}$ reveals a general overestimation in $T_{\delta 18O}$ (Fig. 3). The amount of overestimation in $T_{\delta 18O}$ differs between BL and BH and varies with the applied $\delta^{18}O$-temperature calibration and $\delta^{18}O_{SW}$. In general, the $\delta^{18}O$-temperature calibration of Kim et al.[30] produces $T_{\delta 18O}$ more closely to $T_{\Delta 47}$ than the calibration of Dettmann et al.[29]. Independent from the chosen calibration, the offset between $T_{\delta 18O}$ and $T_{\Delta 47}$ becomes smaller with decreasing $\delta^{18}O_{SW}$. The larges deviations between $T_{\delta 18O}$ and $T_{\Delta 47}$ are observed for BL, showing offsets between 9.4 °C to 11.0 °C for Dettmann et al.[29] and 4.3 °C to 5.7 °C for Kim et al.[30]. The offset for BH is distinctly smaller, ranging from 3.8 °C to 5.2 °C for Dettman et al.[29], while no deviation between $T_{\delta 18O}$ and $T_{\Delta 47}$ is observed if the calibration of Kim et al.[30] is applied. The difference in the offset of $T_{\delta 18O}$ and $T_{\Delta 47}$ between the two calibrations apparently relies in their underlying fractionation factors. The general reduction of the overestimation in $T_{\delta 18O}$ with decreasing $\delta^{18}O_{SW}$, however, reveals that the isotopic composition of the sea water in the Paris Basin must have been lighter that the global mean, as previously assumed. Furthermore, the reduced offset between $T_{\delta 18O}$ and $T_{\Delta 47}$ from BH to BL exhibits short-term variations in $\delta^{18}O_{SW}$ on a seasonal scale. Considering such paleo-environment with seasonal changes in the isotopic composition of the sea water, e.g., through reoccurring of isotopically lighter fresh water influx, shell $\delta^{18}O_C$ variations do not solely reflect variations in SST, leading to an overestimation in $T_{\delta 18O}$ and thereby in MAT and MART. As previously discussed, *Venericor* species occur in environments with considerable variations of fresh water input and are able to tolerate certain changes in salinity[7,8,26]. Ivany et al.[7] estimated the effect of temperature and changes in $\delta^{18}O_{SW}$ on the shell $\delta^{18}O_c$ for *Venericor hatcheplata* from the Eocene Mexican Gulf coast, finding that only ~20% of their observed variations in $\delta^{18}O_C$ are derived from seasonal temperature changes, with the greater amount of the isotopic variability attributable to changes in $\delta^{18}O_{SW}$ induced by the enhanced input of isotopically lighter fresh water.

Seasonal variability in seawater isotopic composition

The $\delta^{18}O_{SW}$ value needed for the temperature calculation for paleo-environmental reconstructions from $\delta^{18}O_C$ is usually estimated through additional methods or archives, like clumped isotopes, Mg/Ca or from tooth apatite and climate models[13,15,32,35]. Previously established $\delta^{18}O_{SW}$ values for the Eocene are predominantly derived from combined $\delta^{18}O$ and Mg/Ca measurements of foraminifera[12–14]. However, these estimates reflect a mean global isotopic seawater composition and thereby are less applicable for a seasonal dynamic shallow marine environment, like the Paris Basin.

For the Paleo North Sea and its adjacent basins, a $\delta^{18}O_{SW}$ value down to ~−3.0‰ is inferred by modelled and proxy data[35,36], distinctly lower than the previously applied −0.75‰ to −1.0‰[6,20,33]. The $\delta^{18}O_{SW}$ values of the Paleo North Sea area, however, also show considerable spatiotemporal heterogeneities. Marchegaino and John[34] reconstructed $\delta^{18}O_{SW}$ values for the Hampshire Basin through the early Bartonian, observing a variation of 0.75‰ to −2.96‰, while Clark et al.[25] estimated the difference in $\delta^{18}O_{SW}$ between the Paris and the Hampshire Basin to be ~2.0‰ during the late Lutetian. Inserting our $T_{\Delta 47}$ and the corresponding $\delta^{18}O_C$ into the calibrations of Dettmann et al.[29] and Kim et al.[30], results in $\delta^{18}O_{SW}$ values of −2.6‰ and −1.8‰ for BL, respectively, −1.7‰ and −0.9‰ for BH (Fig. 4, Supplementary Data 7). Both calibrations reveal a minimum sub-annual variation of the mean isotope composition of the sea water of 0.9‰, which is slightly less than the previously reported annual variability in $\delta^{18}O_{SW}$ from recent and fossil shallow marine environment of 1.0‰ to over 3.0‰[7,11,15]. However, due to the sampling resolution, which covers only half of the observed variability in $\delta^{18}O_C$, the actual annual amplitude is potentially larger.

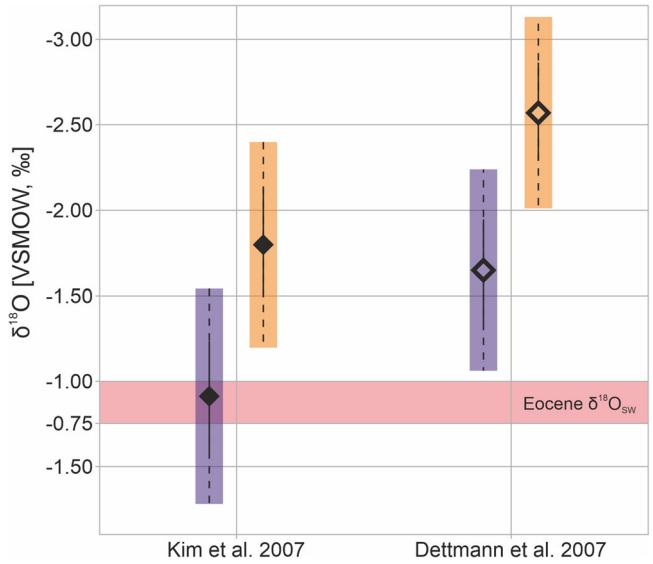

Fig. 4 | Reconstruction of the seasonal variability in the oxygen isotopic composition of the sea water. Calculated $\delta^{18}O_{SW}$ values of summer (BL - orange box) and winter (BH - dark blue box) are displayed in respect to the employed carbonate-water-fractionation calibration (Dettmann et al.[29] – open symbols, Kim et al.[30] – filled symbols). Displayed error bars for the reconstructed $\delta^{18}O_{SW}$ values are derived from the propagated errors of the Δ_{47} measurements and shown as 68% (solid line) and 95% (dashed line) confidence intervals. The red bar marks the commonly used $\delta^{18}O_{SW}$ range for temperature reconstruction in the Eocene Paris Basin.

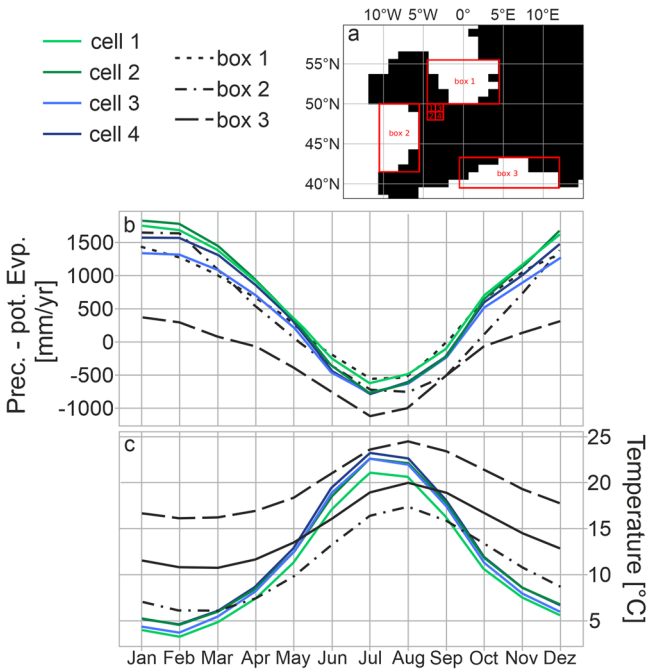

Fig. 5 | Climate model results from within and around the Paris Basin. Seasonal distribution of (**b**) air temperature and (**c**) precipitation minus evapotranspiration for (**a**) three marginal seas (box 1–3) and four continental regions (cell 1–4) derived from the simulated temperature and precipitation of Li et al.[22] using the Community Earth System Model (CESM1.2.2).

The relation between the oxygen isotope composition of the sea water and its salinity is usually described by empirical $\delta^{18}O_{SW}$-salinity-relationships based on linear regression models. However, these relationships can be very different in terms of reconstructing absolute salinity values depending on the oceanic region. Therefore, only relative salinity changes can be derived from the reconstructed $\delta^{18}O_{SW}$ variations. For the modern North Sea relative $\delta^{18}O_{SW}$-salinity-ratios range from 0.27‰/PSU to 0.34‰/PSU[37,38]. Translating the observed seasonal difference of 0.9‰ in $\delta^{18}O_{SW}$ into salinity changes employing these empirical ratios results in a minimum annual shift between 2.5 PSU to 3.3 PSU. This value fits well within the range of 1.5–6.8 PSU for seasonal salinity changes reported for recent marine environments with depth below 30 m[39–41]. For example, in the modern southern North Sea (Knokke, Belgium), Gillikin et al.[42] observed an annual variation of ~5.0 PSU.

The obtained seasonal variability in salinity and the tendency of $\delta^{18}O_{SW}$ to lighter values in comparison to the proposed Eocene global mean of −0.75‰ to −1.0‰, suggest an annual reoccurrence of enhanced fresh water influx (precipitation/riverine input) into the study area. An estimation on the full magnitude and seasonal distribution of this freshening and its influence on the annual $\delta^{18}O_{SW}$ variations is limited, due to the low temporal resolution of the clumped isotope data. For disentangling the effects of temperature and fresh water on the isotopic composition of the carbonate in more detail, additional clumped isotope measurements along the shell would be required.

Comparison of climate model and proxy data

Here we compare annual air temperatures for 40 Ma and 4.9× pre-industrial CO_2 concentration simulated with the Community Earth System Model (CESM1.2.2) using the dataset of Li et al.[22] with our proxy-derived seasonal variations in SST. In addition, simulated precipitation minus potential evapotranspiration is used as indicator for the distribution of annual run-off and compared to the observed seasonal fresh water input inferred by the isotopic data. Four individual model cells (Cell 1–4) located at the paleogeographical position of the Paris Basin and three larger boxes (Box 1–3), which encompass several model cells and represent marginal sea basins around the study area were examined (Fig. 5, Supplementary Data 8).

Cells 1 to 4 are continental cells, as the model resolution is not sufficient to display such a small and shallow marginal sea as the Paris Basin. The four cells are similar in their simulated air temperatures with a MAT of ~11.5 °C and a MART of ~18 °C and thereby exhibit much colder MAT and a distinct larger temperature seasonality as inferred by our and previous proxy reconstruction[5,6,9,20]. The three adjacent marginal sea basins exhibit a smaller MART of ~10 °C, much closer to the proxy-derived annual temperature amplitude. However, their MAT are also considerably colder, ranging from ~10 °C for Box 1, which is directly adjacent to Cells 1–4, to ~19 °C for Box 3 with the larges distance to the study area.

The four cells and three boxes are similar in their pattern for the seasonal distribution of precipitation minus potential evapotranspiration with wet winters and dry summers (Supplementary Fig. S5), suggesting main run-off during the cold season. In contrast, our obtained isotopic data show a strengthen in freshwater input with increasing seasonal temperatures. Considering that the calculated $\delta^{18}O_{SW}$ becomes lighter with rising seasonal temperatures, as deduced from the offset between $T_{\delta 18O}$ and $T_{\Delta 47}$, the influence of isotopically lighter fresh water is most evident during the summer. Such enhanced summer run-off had been shown before from the Mexican Gulf Coast for the early Eocene[7,8]. An enhanced winter run-off as indicated by the model would only be compatible with the measured isotopic signal, if almost no annual temperature variability were assumed and $\delta^{18}O_C$ variations were associated exclusively with the fresh water influx. However, this scenario is rather unlikely, due to a considerable change in solar insolation in the mid-latitudes inducing certain variation in temperature during the year.

The large discrepancy between the proxy and the model data can be attributed to different causes. Albeit, that the CESM is generally considered to be a model that simulates global mean surface temperatures and meridional temperature gradients particularly close to proxy-derived estimates[43], the simulations are still known to generate temperatures that are lower than proxy reconstructions for the mid-latitudes[22]. Since generally lower mean annual temperatures can be associated with greater seasonal temperature variability the greater temperature variability in the simulations compared to the variability in the proxy reconstructions seems consistent

with the lower simulated temperatures compared to the temperatures from the proxy reconstructions. Another aspect is the difference in spatio-temporal resolution between model simulation and proxy record, which might limit the comparability. The obtained isotope record encompasses about seven years, while the used model data is only available for time slices in 10 million year intervals and is an average value over the last 100 years of an equilibrium climate simulation for the 40-million-year time slice. Furthermore, the paleo-geographical reconstruction, which is used for the simulation, is not able to resolve a narrow and shallow marine area like the Paris Basin. The difference in the annual distribution of the simulated precipitation minus evapotranspiration and proxy-derived fresh water influx is therefore potentially induced by comparing a dynamic local signal with a long-term regional average[3].

Conclusion

In this study we used seasonal-target sampling along a seasonal $\delta^{18}O_C$ record of a bivalve shell to obtain the first dual clumped isotope measurements with a sub-annual resolution. We show that the bivalve *V. planicosta* precipitates shell aragonite in clumped isotope equilibrium, thus Δ_{47} values alone may be used to accurately reconstruct growth temperature. The reconstructed SSTs are on the high-end of previously observed MAT for the southern Paleo North Sea during the middle Eocene and show a smaller MART than that inferred from proxy or model data[9,20,22,34]. Moreover, the reconstructed seasonal variability in the $\delta^{18}O_{SW}$ implies enhanced freshwater influx in the study area during the summer months, in contrast to the predicted hydrological conditions derived from climate modelling[22]. Our reconstruction thereby sheds new light on regional climate dynamics of western Europe during the Eocene, revealing hot and wet summer conditions.

We therefore advocate the use of dual-clumped isotope measurements, as demonstrated in this study, to detect potential kinetic effects on the Δ_{47}-based temperature reconstruction. Furthermore, we encourage the combined usage of seasonal-resolved stable isotopes with seasonal-targeted (dual)-clumped isotope analysis to account for sub-annual variations in $\delta^{18}O_{SW}$ and thereby increasing the resolution of future paleo-environmental reconstructions.

Method and material

Sample Material and paleo-environment

Fossil bivalve of the species *Venericor planicosta* (Lamarck), which formed an aragonitic shell and lived as semi-infaunal suspension feeders in a shallow marine environment[27], was employed as an archive. Species of *Venericor* were widespread and abundant along the southern Paleo-North Sea as well as along the Mexican Gulf Coast during the Eocene and have already been used for paleo-environmental reconstructions in several studies[5,7,8,24,26,44,45]. The specimen for the current study was selected from the scientific collection of the Natural History Museum in London. The shell originates form the lower section of the geological site "Le Guépelle" near the village Saint Witz to the north of Paris (49.0841N, 2.538 E). The Eocene paleo-latitudinal position of the sample location was about 7° to 14° further south than todays, depending on the used tectonic model[46–48]. The outcrop consists of shallow marine (water depth <20 m) calcareous sandstone of the "Sables de Guépelle" Formation, which were formed during the Lutetian-Bartonian transition[20,21,49,50]. During this period the area of northern France was characterised by a shallow marine arm of the sea adjacent to the Paleo-North Sea and North Atlantic[24].

Preservation and sampling

To match the relatively large demand on sample material for the dual clumped measurements (50–100 mg) and to meet the requirements for different analytical techniques, several slabs were cut out of the shell parallel to the maximum growth axis. In this process, five 3–7 mm thick-sections, which were ground to remove saw marks, and one polished 150 µm thin-section were prepared.

The polished thin-section was analysed prior to the isotope sampling to determine the preservation state of shell carbonates using cathodoluminescence and Raman-spectroscopy. Unaltered carbonate shells typically exhibit only a dim luminescence with a wave length ~400 nm (blue). Diagenetic alteration and associated incorporation of Mn2+ in the shell results in the shift to longer wave lengths (~580 nm in aragonite, green) and a brighter luminescence[51,52]. Cathodoluminescence microscopy was carried out at the Department of Geography and Geosciences at the Friedrich-Alexander-University in Erlangen (Germany) using a Technosyn cold cathode mounted to a reflective light microscope with a digital camera (Leica Metallux 3, Zeiss AxioCam MRc 5). In addition, we used Raman-spectroscopy to analyse the crystal structure of the shell material and to identify potential recrystallisation. Raman analyses were performed at the Institute for Geoscience at the Goethe University in Frankfurt a.M., (Germany), using a WITec alpha 300 R confocal micro-Raman microscope. For the measurements the excitation laser (532 nm) was operated at 20–40 mW with an integration time of 0.2 s, 10 total accumulations and a holographic grating of 600 grooves mm^{-1}. Both methods reveal a pristine preservation of the shell material, showing a dim, blue luminescence and Raman-spectra, which indicate aragonitic crystal structures in the sampled shell material (Supplementary Fig. S3).

After the preservation screening, one of the thick-sections was etched with Mutvei's solution[53] (25 min at 40 °C) and photographed with a digital camera (Canon EOS 2000D) mounted on a reflective light microscope (ZEISS SteREO Discovery.V8) combined with a sectoral dark field (Schott VisiLED) to identify the growth increments. Increment width was measured using the software FIJI[54] and subsequent utilised for generating a growth model. Applying the growth model to the four records, which were drilled along the remaining thick-sections, enables the superimposing of the gathered isotopic data and the compilation of a master record. Growth model calculation and the tuning of stable isotope data to this model was performed with the software ACYCLE[55].

The remaining four thick-sections (PBB1 to PBB4) were sampled for stable and clumped isotope measurements as shown in Supplementary Fig. S4. Material from the four parallel shell planes was sampled using a micromill (New Wave - Merchantek) equipped with a cylindrical, diamond-coated drill bit (300 µm in diameter). The milling was performed with a fast scan speed (50 µm/s) and a moderate drill speed (70%) to avoid the conversion of the shell aragonite to calcite by friction heating[56,57]. The sampled powder was occasionally tested for its mineralogy using FTIR-spectroscopy, in order to ensure that the selected milling settings do not alter the mineralogical composition of the sample material. FTIR measurements were conducted with a Bruker Alpha II, revealing aragonitic preservation of the milled material.

The sampling was performed in the inner shell, due to a simpler geometry of the increments in this shell part in comparison to the outer shell or hinge plate. This allows an easier visible tracking of the increments, as well as, longer and deeper drilling to match the required material amount while reducing the likelihood of erroneously cutting into a neighbouring increment. To test if there is an isotopic fractionation between the outer and inner shell area, the hinge plate of the section PBB1 was sampled as well.

The sampling for the stable isotopes analysis was conducted by drilling parallel to the increments and in growth direction, continuously abrading the material with a width and sampling depth of 150 µm.

Two of the before sampled thick-sections (PBB3 and PBB4) were then selected for the dual clumped isotope measurements. These two sections revealed the most favourable shell geometry for the drilling and emerged from the same saw cut, which enables mirrored sampling and thus improves the comparability of the drilling profiles. Four to five tracks along the full length of the inner shell were drilled, parallel to the increments. The master record of the stable oxygen isotope analysis was employed to choose sampling positions characterised by seasonal extrema. Positions along the last four years of the two shell planes were chosen, allowing the longest tracks. However, in this shell area the increments are also distinctly closer together, which results in occasionally missing the aimed record extrema, due to the limitations of the drill equipment. The drilling was conducted using the full drill diameter and a sampling depth of 750 µm, which was achieved by

increasing the drilling depth in 150 µm steps in repeating passes. After each drilling pass the milled carbonate powder was weighted and stored separately. In addition, two to three stable isotope samples were taken from the gathered material as control samples to determine the internal variability of each drilling pass and monitor potential changes in isotopic composition with increasing sampling depth enabling to match the stable and clumped isotope records. The selection of the material for the dual clumped analysis was based on the $\delta^{18}O$ results of the control samples, discarding outliers or drilling passes with a high internal variability.

Isotopic measurements

All isotope measurements were conducted at the Institute for Geoscience at the Goethe University in Frankfurt a.M., Germany. For the analysis of stable isotopes 80 to 120 µg of the carbonate powder was reacted with 100% phosphoric acid at 72 °C in a He atmosphere. The evolving CO_2 was measured with a Finnigan Gas Bench coupled to Finnigan MAT 253 mass spectrometer. All data is displayed in δ notation and expressed in per mill relative to the Vienna-Pee Dee Belemnite standard (‰, VPDB). A Carrara marble (calibrated to NBS-19) was measured along with the samples as calibration standard and for monitoring the reproducibility of the analysis, yielding analytical precision of <0.07‰ for $\delta^{18}O$ and <0.05‰ $\delta^{13}C$ for al sample runs. The subsequent conversion of the isotopic data into temperature values and sea water isotopic composition was carried out using the R package "isogeochem"[58,59]. Resulting $\delta^{18}O_{SW}$ values are given in per mill relative to the Vienna Standard Mean Ocean Water (‰, VSMOW).

For the investigation of the dual clumped isotope composition of the shell material, we selected drilled carbonate powder from ten sampling tracks (covering 41 drilling passes), based on the $\delta^{18}O$ values of the control samples. The material of five tracks was pooled to produce two bulk samples, one covering the isotopically lighter and one the isotopically heavier section of the $\delta^{18}O$ record. Total weight per sample was sufficient to yield seven replicates for dual clumped isotope analysis.

The dual clumped analysis ($\Delta_{47} + \Delta_{48}$) were carried out following the methodology described in Bernecker et al.[60]. Samples and carbonate standards, ETH-1, ETH-2 and ETH3, were weighted into 10.0 ± 0.2 mg aliquots and digested in 107-108%wt phosphoric acid at 90 °C. A carbonate standard was analysed after every third sample. To facilitate transfer of mass spectrometric raw data to the Carbon Dioxide Equilibrium Scale (CDES), carbon dioxide of three distinct bulk isotope composition, equilibrated at 25 °C and 1000 °C, were measured at least once a week, totalling in 6 equilibrated gasses analysed per week. Before introduction to the mass-spectrometer, sample and standard CO_2 was purified to remove any contaminants and residual water, using an in-house gas purifications system HAL[16]. The purified CO_2 was analysed against a working gas ($\delta^{13}C_{VPDB} = 4.20‰$, $\delta^{18}O_{VSMOW} = 25.26‰$) on a Thermo Scientific 253 plus mass spectrometer adjust to an intensity of 16000 ± 100 mV on m/z 44. Measurements were carried out as 13 acquisitions, where each acquisition includes 10 cycles with an integration time of 20 s each, facilitating a total integration time of 2600 s per replicate. Within these conditions the shot noise limited corresponds to 0.024‰ for Δ_{48} and 0.007‰ for Δ_{47}[61].

Data processing

A nonlinear least-squares model was applied to the $\delta^{18}O$ record, to detect the general seasonal variation and to minimise the influence of potential noise. Following that, except in the low latitudes, the seasonal temperature pattern is predominantly determined by the annual solar insulation, a sinusoidal function was fitted to the master record data. The mean sine position (M) and the amplitude (A) of the resulting sine wave were used to determine the annual mean, respectively, the seasonal amplitude of $\delta^{18}O$[7,62].The R code for the curve fitting, as well as, a summary of the quality of the model fit is given in the supplements[59].

The clumped isotope data were processed following the method described in Bernecker et al.[60]. Measured intensities of the half-mass m/z 47.5 of the equilibrated gases at 25 °C and 1000 °C were first employed to derive scaling factors for non-linearity correction, assuming that the slopes of δ_{47} vs Δ_{47} and δ_{48} vs Δ_{48} should be indistinguishable from zero[23]. Data were then corrected in D47crunch[63] using the "pooled session" approach, as all of the replicates of both samples were measured in the same session, with drift correction applied. D47crunch[63] furthermore reports fully error-propagated uncertainties. A summary of the analytical, calibration and resulting propagated errors are displayed in Table 1. As there are currently no carbonate standards with an accepted Δ_{48} value, heated and equilibrated gases were selected as anchors with assigned Δ_{47} and Δ_{48} values of 0.9196 and 0.345‰, respectively, for CO_2 equilibrated at 25 °C, and values of 0.0266 and 0‰ for CO_2 equilibrated at 1000 °C. Dual clumped isotope data are therefore reported in CDES[64] and for a reaction temperature of 90 °C (CDES 90). Δ_{47} (CDES 90) and Δ_{48} (CDES 90) were further compared to the CDES 90 calibration of Fiebig et al.[23] to account for potential disequilibrium of the sample material.

The simultaneously measured stable isotope data ($\delta^{18}O$, $\delta^{13}C$) were also corrected using D47crunch[63] based on accepted values of the reference material ETH-1, ETH-2 and ETH-3[65]. As with the previous isotope data, the values are reported relative to the Vienna-Pee Dee Belemnite standard (VPDB). For the $\delta^{18}O$ data an acid fractionation factor of 1.008541 at 90 °C[66] has been applied, to account for isotopic fractionation induced by acid digestion.

For carbonate formation temperature calculation, the Δ_{47}-temperature calibration of Fiebig et al.[23] was employed. The temperatures were also comparatively calculated using the Δ_{47}-temperatures calibration of Daëron & Vermeesch[67], yielding about 1 °C colder values. However, the resulting temperature values of both calibrations are statistically indistinguishable (Supplementary Fig. S6, Supplementary Data 4).

Analysis of climate model data

We use surface temperature and precipitation output from published climate model simulations for 40 Ma[22], run with the coupled climate model CESM1.2.2. The solar constant was set to 1344.67 Wm^{-1}, based on a linear increase from 1302 Wm^{-1} at 540 Ma to 1361 Wm^{-1} at present, present values of orbital parameters are used and the palaeogeography is based on the paleo-digital elevation model[68]. The simulation was done in two steps: the fully coupled model with a horizontal resolution of approximately 4° × 4° was used to reach an equilibrium close to reconstructed global mean surface temperatures of 19.8 °C by tuning the atmospheric CO_2 concentration to 1372 ppm. Based on this simulation the atmosphere-land-coupled version of the model is used on a finer horizontal resolution of approximately 1° × 1° to simulate 100 years. For details, see Li et al.[22].

Potential Evapotranspiration (PET) was calculated using the Thornthwaite equation[69] with simulated temperatures T:

$$E_p = \begin{cases} 0 & if\ T < 0 \\ 16 \cdot \frac{L}{360} \cdot \left(\frac{10 \cdot T}{I}\right)^a & if\ 0 \le T \le 26\ ^\circ C \\ -415.85 + 30.24 \cdot T - 0.43 \cdot T^2 & if\ T > 26\ ^\circ C \end{cases} \quad (1)$$

with

$$a = 6.75 \cdot 10^{-7} \cdot I^3 - 7.71 \cdot 10^{-5} I^2 + 1.79 \cdot 10^{-2} \cdot I + 0.49, \quad (2)$$

$$I = \Sigma \left(\frac{T}{5}\right)^{1.514} \text{ for months with } T > 0\ ^\circ C. \quad (3)$$

Data availability

Extended data and calculations belonging to this study are summarised in the supplementary material and can be accessed on the Zenodo database (https://zenodo.org/records/11394638). These supplements contain the following supplementary data files:

- Supplementary material: Supplementary Figs. Fig. S1 to Fig. S6
- Supplementary data 1: Stable isotopes control samples
- Supplementary data 2: Stable isotopes inner shell record

- Supplementary data 3: Non-linear regression model
- Supplementary data 4: Temperature calculations
- Supplementary data 5: Recalculated temperatures "Le Guépelle"
- Supplementary data 6: Offsets between stable and clumped isotope temperatures
- Supplementary data 7: Recalculated $\delta^{18}O_{SW}$
- Supplementary data 8: Climate model data output
- Supplementary data 9: Summary of clumped isotope data including replicates for samples, standards and heated gases
- Supplementary data 10: File contains CESM data output and employed Python code for data extraction
- Supplementary data 11: R script non-linear regression model

Code availability

Python script was used to extract climate data from the CESM simulation. In addition to standard python package, the geoutils package was used. The employed code and corresponding descriptions are provided in the climate model supplement. The non-linear regression model was computed using a R script (supplementary data 11). All code scripts can be accessed on the Zenodo database (https://zenodo.org/records/11394638).

Received: 30 January 2024; Accepted: 5 June 2024;
Published online: 15 June 2024

References

1. Tierney, J. E. et al. Past climates inform our future. *Science* **370**, https://doi.org/10.1126/science.aay3701 (2020).
2. Zachos, J. C., Dickens, G. R. & Zeebe, R. E. An early Cenozoic perspective on greenhouse warming and carbon-cycle dynamics. *Nature* **451**, 279–283 (2008).
3. Ivany, L. C. & Judd, E. J. Deciphering Temperature Seasonality in Earth's Ancient Oceans. *Annu. Rev. Earth Planet. Sci.* **50**, 123–152 (2022).
4. Lunt, D. J. et al. Warm climates of the past-a lesson for the future? *Philos. Trans. Ser. A Math. Phys. Eng. Sci.* **371**, 20130146 (2013).
5. Andreasson, F. P. & Schmitz, B. Winter and summer temperatures of the early middle Eocene of France from Turritella δ18O profiles. *Geol* **24**, 1067 (1996).
6. Andreasson, F. P. & Schmitz, B. Temperature seasonality in the early middle Eocene North Atlantic region: Evidence from stable isotope profiles of marine gastropod shells. *Geol. Soc. Am. Bull.* **112**, 628–640 (2000).
7. Ivany, L. C. et al. Intra-Annual Isotopic Variation in Venericardia Bivalves: Implications for Early Eocene Temperature, Seasonality, and Salinity on the U.S. Gulf Coast. *J. Sediment. Res.* **74**, 7–19 (2004).
8. Keating-Bitonti, C. R., Ivany, L. C., Affek, H. P., Douglas, P. & Samson, S. D. Warm, not super-hot, temperatures in the early Eocene subtropics. *Geology* **39**, 771–774 (2011).
9. Winter, N. J. et al. The Giant Marine Gastropod Campanile Giganteum (Lamarck, 1804) as a High-Resolution Archive of Seasonality in the Eocene Greenhouse World. *Geochem. Geophys. Geosyst*. **21**, https://doi.org/10.1029/2019GC008794 (2020).
10. Zhang, J. Z., Petersen, S. V., Winkelstern, I. Z. & Lohmann, K. C. Seasonally Variable Aquifer Discharge and Cooler Climate in Bermuda During the Last Interglacial Revealed by Subannual Clumped Isotope Analysis. *Paleoceanogr. Paleoclimatol.* **36**, https://doi.org/10.1029/2020PA004145 (2021).
11. Zhang, J. Z. & Petersen, S. V. Clumped and oxygen isotope sclerochronology methods tested in the bivalve Lucina pensylvanica. *Chem. Geol.* **620**, 121346 (2023).
12. Shackleton, N. J. & Kennett, J. P. Paleotemperature History of the Cenozoic and the Initiation of Antarctic Glaciation: Oxygen and Carbon Isotope Analyses in DSDP Sites 277, 279 and 281. *Initial Rep. Deep Sea Drill. Proj.* **29**, 743–755 (1975).
13. Lear, C. H., Elderfield, H. & Wilson, P. A. Cenozoic deep-Sea temperatures and global ice volumes from Mg/Ca in benthic foraminiferal calcite. *Science* **287**, 269–272 (2000).
14. Zachos, J. C., Stott, L. D. & Lohmann, K. C. Evolution of Early Cenozoic marine temperatures. *Paleoceanography* **9**, 353–387 (1994).
15. Winter, et al. Absolute seasonal temperature estimates from clumped isotopes in bivalve shells suggest warm and variable greenhouse climate. *Commun. Earth Environ*. **2**, https://doi.org/10.1038/s43247-021-00193-9 (2021).
16. Fiebig, J. et al. Combined high-precision Δ48 and Δ47 analysis of carbonates. *Chem. Geol.* **522**, 186–191 (2019).
17. Bajnai, D. et al. Dual clumped isotope thermometry resolves kinetic biases in carbonate formation temperatures. *Nat. Commun.* **11**, 4005 (2020).
18. Davies, A. J. et al. Dual clumped isotope thermometry of coral carbonate. *Geochim. Cosmochimica Acta* **338**, 66–78 (2022).
19. Davies, A. J. et al. Isotopic disequilibrium in brachiopods disentangled with dual clumped isotope thermometry. *Geochim. Cosmochimica Acta* **359**, 135–147 (2023).
20. Huyghe, D., Lartaud, F., Emmanuel, L., Merle, D. & Renard, M. Palaeogene climate evolution in the Paris Basin from oxygen stable isotope (δ 18 O) compositions of marine molluscs. *JGS* **172**, 576–587 (2015).
21. Gely, J. P. & Lorenz, C. Analyse séquentielle de l'Eocène et de l'Oligocène du bassin Parisien (France). *Rev. Inst. Fr. Pét.* **46**, 713–747 (1991).
22. Li, X. et al. A high-resolution climate simulation dataset for the past 540 million years. *Sci. Data* **9**, 371 (2022).
23. Fiebig, J. et al. Calibration of the dual clumped isotope thermometer for carbonates. *Geochim. Cosmochimica Acta* **312**, 235–256 (2021).
24. Huyghe, D., Merle, D., Lartaud, F., Cheype, E. & Emmanuel, L. Middle Lutetian climate in the Paris Basin: implications for a marine hotspot of paleobiodiversity. *Facies* **58**, 587–604 (2012).
25. Clark, A. J., Vellekoop, J. & Speijer, R. P. Hydrological differences between the Lutetian Paris and Hampshire basins revealed by stable isotopes of conid gastropods. *BSGF Earth Sci. Bull.* **193**, 3–15 (2022).
26. Sessa, J. A., Ivany, L. C., Schlossnagle, T. H., Samson, S. D. & Schellenberg, S. A. The fidelity of oxygen and strontium isotope values from shallow shelf settings: Implications for temperature and age reconstructions. *Palaeogeogr. Palaeoclimatol. Palaeoecol.* **342–343**, 27–39 (2012).
27. Todd, J. A. & Harper, E. M. Stereotypic boring behaviour inferred from the earliest known octopod feeding traces: Early Eocene, southern England. *LET* **44**, 214–222 (2011).
28. Grossman, E. L. & Ku, T.-L. Oxygen and carbon isotope fractionation in biogenic aragonite: Temperature effects. *Chem. Geol.: Isot. Geosci. Sect.* **59**, 59–74 (1986).
29. Dettman, D. L., Reische, A. K. & Lohmann, K. C. Controls on the stable isotope composition of seasonal growth bands in aragonitic fresh-water bivalves (unionidae). *Geochim. Cosmochimica Acta* **63**, 1049–1057 (1999).
30. Kim, S.-T., O'Neil, J. R., Hillaire-Marcel, C. & Mucci, A. Oxygen isotope fractionation between synthetic aragonite and water: Influence of temperature and Mg2+ concentration. *Geochim. Cosmochimica Acta* **71**, 4704–4715 (2007).
31. Daëron, M. et al. Most Earth-surface calcites precipitate out of isotopic equilibrium. *Nat. Commun.* **10**, 429 (2019).
32. Walliser, E. O. et al. The bivalve Glycymeris planicostalis as a high-resolution paleoclimate archive for the Rupelian (Early Oligocene) of central Europe. *Clim* **11**, 653–668 (2015).
33. Kelson, J. R., Petersen, S. V., Niemi, N. A., Passey, B. H. & Curley, A. N. Looking upstream with clumped and triple oxygen isotopes of estuarine oyster shells in the early Eocene of California, USA. *Geology* **50**, 755–759 (2022).

34. Marchegiano, M. & John, C. M. Disentangling the Impact of Global and Regional Climate Changes During the Middle Eocene in the Hampshire Basin: New Insights From Carbonate Clumped Isotopes and Ostracod Assemblages. *Paleoceanog and Paleoclimatol* **37**, https://doi.org/10.1029/2021PA004299 (2022).
35. Zhu, J. et al. Simulation of early Eocene water isotopes using an Earth system model and its implication for past climate reconstruction. *Earth Planet. Sci. Lett.* **537**, 116164 (2020).
36. Zacke, A. et al. Surface-water freshening and high-latitude river discharge in the Eocene North Sea. *JGS* **166**, 969–980 (2009).
37. Harwood, A. J., Dennis, P. F., Marca, A. D., Pilling, G. M. & Millner, R. S. The oxygen isotope composition of water masses within the North Sea. *Estuar. Coast. Shelf Sci.* **78**, 353–359 (2008).
38. Scheurle, C. & Hebbeln, D. Stable oxygen isotopes as recorders of salinity and river discharge in the German Bight, North Sea. *Geo Mar. Lett.* **23**, 130–136 (2003).
39. Morimoto, M. et al. Salinity records for the 1997–98 El Niño from Western Pacific corals. *Geophys. Res. Lett*. **29**, https://doi.org/10.1029/2001GL013521 (2002).
40. Surge, D. M. & Lohmann, K. C. Temporal and spatial differences in salinity and water chemistry in SW Florida estuaries: Effects of human-impacted watersheds. *Estuaries* **25**, 393–408 (2002).
41. Watanabe, T., Winter, A. & Oba, T. Seasonal changes in sea surface temperature and salinity during the Little Ice Age in the Caribbean Sea deduced from Mg/Ca and 18O/16O ratios in corals. *Mar. Geol.* **173**, 21–35 (2001).
42. Gillikin, D. P. et al. Barium uptake into the shells of the common mussel (Mytilus edulis) and the potential for estuarine paleo-chemistry reconstruction. *Geochim. Cosmochimica Acta* **70**, 395–407 (2006).
43. Lunt, D. J. et al. DeepMIP: model intercomparison of early Eocene climatic optimum (EECO) large-scale climate features and comparison with proxy data. *Clim* **17**, 203–227 (2021).
44. Purton, L. M. A., Shields, G. A., Brasier, M. D. & Grime, G. W. Metabolism controls Sr/Ca ratios in fossil aragonitic mollusks. *Geology* **27**, 1083–1086 (1999).
45. Purton, L. M. A. & Brasier, M. D. Giant protist Nummulites and its Eocene environment: Life span and habitat insights from δ18O and δ13C data from Nummulites and Venericardia, Hampshire basin, UK. *Geology* **27**, 711 (1999).
46. van Hinsbergen, D. J. J. et al. A Paleolatitude Calculator for Paleoclimate Studies. *PloS One* **10**, e0126946 (2015).
47. Doubrovine, P. V., Steinberger, B. & Torsvik, T. H. Absolute plate motions in a reference frame defined by moving hot spots in the Pacific, Atlantic, and Indian oceans. *J. Geophys. Res*. **117**, https://doi.org/10.1029/2011JB009072 (2012).
48. Besse, J. & Courtillot, V. Apparent and true polar wander and the geometry of the geomagnetic field over the last 200 Myr. *J. Geophys. Res*. **107**, https://doi.org/10.1029/2000JB000050 (2002).
49. King, C. *A revised correlation of Tertiary rocks in the British Isles and adjacent areas of NW Europe* (The Geological Society, Bath UK, 2016).
50. Dominici, S. & Zuschin, M. Palaeocommunities, diversity and sea-level change from middle Eocene shell beds of the Paris Basin. *JGS* **173**, 889–900 (2016).
51. Götze, J. Application of cathodoluminescence microscopy and spectroscopy in geosciences. *Microsc. Microanal.* **18**, 1270–1284 (2012).
52. Barbin, V. Application of cathodoluminescence microscopy to recent and past biological materials: a decade of progress. *Min. Pet.* **107**, 353–362 (2013).
53. Schöne, B. R., Dunca, E., Fiebig, J. & Pfeiffer, M. Mutvei's solution: An ideal agent for resolving microgrowth structures of biogenic carbonates. *Palaeogeogr. Palaeoclimatol. Palaeoecol.* **228**, 149–166 (2005).
54. Schindelin, J. et al. Fiji: an open-source platform for biological-image analysis. *Nature methods* **9**, 676–682 (2012).
55. Li, M., Hinnov, L. & Kump, L. Acycle: Time-series analysis software for paleoclimate research and education. *Comput. Geosci.* **127**, 12–22 (2019).
56. Staudigel, P. T. & Swart, P. K. Isotopic behavior during the aragonite-calcite transition: Implications for sample preparation and proxy interpretation. *Chem. Geol.* **442**, 130–138 (2016).
57. Staudigel, P. et al. Fingerprinting Kinetic Isotope Effects and Diagenetic Exchange Reactions Using Fluid Inclusion and Dual-Clumped Isotope Analysis. *Geochem. Geophys. Geosyst.* **24**, https://doi.org/10.1029/2022GC010766 (2023).
58. Bajnai, D. *isogeochem: Tools for Stable Isotope Geochemistry. R package version 1.1.1*, https://davidbajnai.github.io/isogeochem (2023).
59. R Core Team. *R: A Language and Environment for Statistical Computing. Version 4.0.4* (R Foundation for Statistical Computing, Vienna, Austria, 2021).
60. Bernecker, M. et al. A robust methodology for triple (Δ47, Δ48, Δ49) clumped isotope analysis of carbonates. *Chem. Geol.* **642**, 121803 (2023).
61. Merritt, D. A., Hayes, J. M. & Des Marais, D. J. Carbon isotopic analysis of atmospheric methane by isotope-ratio-monitoring gas chromato graphy-mass spectrometry. *J. Geophys. Res.* **100**, 1317–1326 (1995).
62. Wilkinson, B. H. & Ivany, L. C. Paleoclimatic inference from stable isotope profiles of accretionary biogenic hardparts – a quantitative approach to the evaluation of incomplete data. *Palaeogeogr. Palaeoclimatol. Palaeoecol.* **185**, 95–114 (2002).
63. Daëron, M. Full Propagation of Analytical Uncertainties in Δ47 Measurements. *Geochem. Geophys. Geosyst.* **22**, 1–19 (2021).
64. Dennis, K. J., Affek, H. P., Passey, B. H., Schrag, D. P. & Eiler, J. M. Defining an absolute reference frame for 'clumped' isotope studies of CO2. *Geochim. Cosmochimica Acta* **75**, 7117–7131 (2011).
65. Bernasconi, S. M. et al. Reducing Uncertainties in Carbonate Clumped Isotope Analysis Through Consistent Carbonate-Based Standardization. *Geochem. Geophys. Geosyst. G3*, **19**, 2895–2914 (2018).
66. Kim, S.-T., Mucci, A. & Taylor, B. E. Phosphoric acid fractionation factors for calcite and aragonite between 25 and 75 °C: Revisited. *Chem. Geol.* **246**, 135–146 (2007).
67. Daëron, M. & Vermeesch, P. Omnivariant Generalized Least Squares regression: Theory, geochronological applications, and making the case for reconciled Δ47 calibrations. *Chem. Geol.* **647**, 121881 (2024).
68. Scotese, C. R. & Wright, N. M. *PALEOMAP Paleodigital Elevation Models (PaleoDEMS) for the Phanerozoic* (Zenodo).
69. Thornthwaite, C. W. An Approach toward a Rational Classification of Climate. *Geographical Rev.* **38**, 55 (1948).

Acknowledgements

This research was funded through the VeWA consortium by the LOEWE programme of the Hessen Ministry of Higher Education, Research and the Arts, Germany. The authors kindly thank Sven Hofmann for technical support in the laboratory. Furthermore, we thank Michael Joachimski for supporting the cathodoluminescence measurements. The authors also kindly thank Daniel Vigelius for assistance for sample drilling and Raman measurements.

Author contributions

The study was initially conceived by J.F.K., A.J.D, J.F. and J.R. Preservation screening and determination of the growth model was performed by J.F.K. with support of A.W. and S.V. Stable isotope analysis and data processing were carried out by J.F.K. Dual-clumped isotope measurement and data processing was done by A.J.D, M.B. and J.F., while J.B. and T.H. were responsible for anaylsing the climate model data. J.A.T. contributed the sample material. The funding of the study was acquired through J.R. The first

draft of the manuscript was written by J.F.K. and revised with contributions of all authors.

Funding
Open Access funding enabled and organized by Projekt DEAL.

Competing interests
The authors declare no competing interests.

Additional information
Supplementary information The online version contains supplementary material available at https://doi.org/10.1038/s43247-024-01491-8.

Correspondence and requests for materials should be addressed to Jorit F. Kniest.

Peer review information *Communications Earth & Environment* thanks Yongyun Hu and the other, anonymous, reviewer(s) for their contribution to the peer review of this work. Primary Handling Editor: Carolina Ortiz Guerrero. A peer review file is available